ChemCatChem

The European Society Journal for Catalysis

Chemistry Europe

European Chemical Societies Publishing

Supported by GECATS GERMAN CATALYSIS SOCIETY

Accepted Article

Title: Nanoflower-like Cu/SiO2 Catalyst for Hydrogenation of Ethylene Carbonate to Methanol and Ethylene Glycol: Enriching H2 Adsorption

Authors: Mengjiao Zhang, Youwei Yang, Antai Li, Dawei Yao, Yueqi Gao, Busha Assaba Fayisa, Mei-Yan Wang, Shouying Huang, Jing Lv, Yue Wang, and Xinbin Ma

To be cited as: *ChemCatChem* 10.1002/cctc.202000365

Link to VoR: https://doi.org/10.1002/cctc.202000365

WILEY-VCH

Nanoflower-like Cu/SiO_2 Catalyst for Hydrogenation of Ethylene Carbonate to Methanol and Ethylene Glycol: Enriching H_2 Adsorption

Mengjiao Zhang, [a]1 Youwei Yang, [a]1 Antai Li, [a] Dawei Yao, [a] Yueqi Gao, [a] Busha Assaba Fayisa, [a] Mei-Yan Wang, [a] Shouying Huang, [a] Jing Lv, [a] Yue Wang,*[a] and Xinbin Ma*[a]

Dedication [1]M. Zhang and [1]Y. Yang contributed equally to this work.

[a] M. Zhang, Y. Yang, A. Li, Dr. D. Yao, Y Gao, B. A. Fayisa, Dr. M-Y. Wang, Dr. S. Huang, Dr. J. Lv, Dr. Y. Wang, Prof. Dr. X. Ma
Key Laboratory for Green Chemical Technology of Ministry of Education, Collaborative Innovation Centre of Chemical Science and Engineering, School of Chemical Engineering and Technology, Tianjin University
Tianjin 300072 (P. R. China)
E-mail: yuewang@tju.edu.cn, xbma@tju.edu.cn

Abstract: The hydrogenation of ethylene carbonate (EC) to produce methanol and ethylene glycol (EG) is one of the key steps in the promising route for CO_2 utilization on a large scale. However, the high H_2/EC ratio in feed (usually as 200~300) was generally required to achieve favorable catalytic activity, inducing the high cost for H_2 circulation in the industrial application. Here, we report a series of nanoflower-like catalysts with curved fibers and open ends, among which the catalyst with the highest fiber density exhibited nearly 98% EC conversion, 75% methanol selectivity and over 99% EG selectivity when the H_2/EC ratio was decreased to 60. Combining the characterizations of active species distribution and high-pressure H_2 adsorption, it is demonstrated that the nanoflower-like morphology with dense fibers could remarkably enrich the hydrogen adsorption, consequently accelerate the reaction rate and present the excellent performance at a low H_2/EC ratio. These insights may provide instructive suggestions for further design of catalysts for the hydrogenation reactions.

Introduction

Carbon dioxide, being one of the main greenhouse gases, has caused a series of environmental issues with its gradually increasing concentration in the atmosphere.[1-4] Meanwhile, as an economical, safe and renewable carbon resource, carbon dioxide can be used to produce many kinds of organic components, materials and carbohydrates.[5-7] From the viewpoint of resource utilization, developing the synthetic routes from CO_2 for industrial production could be one of the most attractive options. As the simplest saturated mono-carbon alcohol, methanol is not only the basic organic feedstock used in plastics, fine chemicals and petrochemical industries, but also a new type of clean fuel energy with broad application prospect.[8-9] However, because of the thermodynamically stable and inert properties, direct hydrogenation of CO_2 to methanol is restricted to chemical equilibrium, and the single-pass conversion as well as the product selectivity is not satisfying even at harsh and favorable reaction conditions, which hampers its development process in industrialization.[9-12]

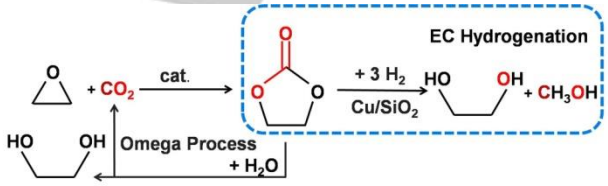

Scheme 1. Utilization of CO_2 with ethylene oxide to produce methanol and EG via EC hydrogenation.

In recent years, the route of carbon dioxide reacting with ethylene oxide to produce ethylene carbonate (EC) which is as an intermediate then hydrogenated to methanol and ethylene glycol (EG) (Scheme 1) has attracted numerous attention from both academics and industry.[13-14] The technique has many advantages in both thermodynamics and kinetics, as well as high atom economy, mild reaction conditions and good selectivity of methanol.[14-19] Moreover, the ethylene oxide could finally be converted to EG in this process, an vital raw material for the synthesis of polyesters and resins[20], further boosting the technological economic efficiency and promising market application. Notably, CO_2 inserting into ethylene oxide to produce EC, as one of the key steps in the omega process (as shown in Scheme 1), is a relative mature technology and has established industrial applications.[15, 21-22] Therefore, the research to explore effective catalysts for EC hydrogenation is of great importance in developing commercial utilization of CO_2.

Homogeneous (PNP) Ru^{II} pincer complex catalysts were reported by Ding and co-workers for the hydrogenation of EC under relative mild conditions, achieving over 99% conversion and selectivity.[15] Zubar and co-workers prepared the first base-metal Mn-PNN complex in the hydrogenation of cyclic organic carbonates, which presented 92% methanol yield and over 99% EG yield in EC hydrogenation.[13] Despite the good catalytic performance, homogeneous catalysts suffer from high cost, difficulty in separation and recovery from the products, making it hard for the large-scale industrial applications. Cu-based catalysts have been wildly used in heterogeneous continuous and selective hydrogenation of C=O/C-O bonds and exhibited good activity and products selectivity.

Great advances in EC hydrogenation have been achieved on Cu-based catalysts. Liu and co-workers investigated the effect of different supports in Cu-catalyzed EC hydrogenation, revealing that excessive surface basicity or acidity of the supports would induce side reactions, and SiO_2 was the most suitable support among those.[18] Concerning the nature of active sites, many studies have reported that the synergy effect of Cu^0 and Cu^+ species was crucial to achieve excellent catalytic performance of Cu/SiO_2 in EC hydrogenation, where the Cu^0 species could facilitate the dissociation of H_2, while the Cu^+ species acted as the Lewis acid sites to activate the EC molecules.[18, 23-26] Cu/HMS catalyst prepared by ammonia evaporation method was applied in the continuous fixed-bed reactor and exhibited 100% EC conversion and 74% methanol selectivity, over 99% EG selectivity.[23] After investigating the evolution of surface active sites on Cu/MCM-41 catalysts with different Cu/Si ratios, Deng et al. suggested that the appropriate surface $Cu^+/(Cu^0+Cu^+)$ ratio of ca.28% might contribute to the optimal catalytic activity.[27] Additionally, doping oxides with intermediate Lewis acidity, which may increase the surface acid concentration to some proper extent, is believed to contribute to the activation of carbonate reactant and enhancing the catalytic performance in EC hydrogenation, such as Cu_8-Mg_1-$Zr_{0.47}/SiO_2$[28] and $Cu/ZrO_x@Al_2O_3$[29] catalysts. Moreover, polyhydroxy compounds have been used in the Cu/SiO_2 catalysts to improve the dispersion of copper species and prolong the life-span. Zhang and co-workers found that modification by β-cyclodextrin could promote the dispersion of active species and hinder the particles aggregation, furnishing the long-time stability.[30] Chen et al. developed a glucose-modified Cu/SiO_2 catalyst for EC hydrogenation with over 500 h life-time, showing that optimal glucose remarkably alleviated the catalyst deactivation and promoted catalytic stability.[16]

However, most reported Cu-based catalysts for EC hydrogenation were used under high partial pressure of hydrogen[13, 15, 17-18, 29] or huge hydrogen-to-ester ratio (ie, the molar ratio of H_2 to EC, denoted as H_2/EC, usually reported between 200~300)[14, 16, 23, 27, 31] to achieve a favorable catalytic performance, which would lead to huge hydrogen circulation flow in the system and increase the costs of recycling compressors and driving power in the potential industrial application. In our previous work, we found out that the catalyst with nanotube-assembled hollow sphere structure could significantly enrich hydrogen adsorption, and exhibited superior catalytic activity in the hydrogenation of dimethyl oxalate even under low hydrogen partial pressure. The hydrogen-to-ester ratio could be reduced from 80 to 20, which was attributed to the enhanced adsorption ability on the concave side of curved surfaces.[32-33] However, when we tried to apply this catalyst for EC hydrogenation, there was still one unavoidable problem. The spatial restriction effect of the nanotubes on the surface of hollow sphere could promote the further hydrogenation in a consecutive reaction[32], which might lead to unsatisfactory selectivity of target products.

Herein, we designed and fabricated a series of nanoflower-like catalysts with curved surfaces and open ends by one-step hydrolysis precipitation method for the hydrogenation of EC to produce methanol and EG, denoted as Cu/SiO_2-F catalysts. To illustrate the effect of nanoflower-like structure on enriching hydrogen adsorption, we further prepared a copper catalyst supported on solid silica spheres for comparison. It is demonstrated that the Cu/SiO_2-F catalyst with the highest fiber density could achieve the nearly 98% EC conversion even under the decreased H_2/EC of 60, which is far lower than that of 200~300 used in literature[23, 27-28, 31], accompanied with the high methanol selectivity of 75% and over 99% EG selectivity. Combining the quantitative characterizations of the surface active species and high-pressure hydrogenation adsorption tests at reaction temperature, it could be concluded that nanoflower-like morphology could significantly enhance the hydrogen adsorption and enrich hydrogen concentration among the fibers, sequentially favorable to the excellent performance under a low H_2/EC ratio in feedstock. These insights may provide practical guidance for further design of catalysts for consecutive hydrogenation reactions.

Results and Discussion

Morphology and Textural Properties of the Catalysts

A series of nanoflower-like silica supported copper-based catalysts were fabricated by using one-step hydrolysis precipitation method, denoted as Cu/SiO_2-F-x, where x means the molar ratio of $(NH_4)_2CO_3$ to copper used in the preparation step. To compare with the nanoflower morphology, silica support of solid sphere structure was applied to prepare the Cu/SiO_2-S catalyst with similar copper loading via modified ammonia evaporation method. In order to characterize whether the designed morphology was synthesized, scanning electron microscopy (SEM) and transmission electron microscopy (TEM) images of the calcined Cu/SiO_2-F and Cu/SiO_2-S samples were measured. As demonstrated in Figure S1, the as-prepared Cu/SiO_2-F samples exhibited the nanoflower-like morphology with special V-type fiber channels with open-ended structure. Meanwhile, the spherical morphology of solid silica support in the Cu/SiO_2-S catalyst was well maintained after the preparation procedures. There are no obvious channels observed but a lot of small interlaced flakes appeared and stacked on the sphere surface, indicating the formation of lamellar copper silicate.[32, 34]

TEM images at high magnifications were further conducted. As illustrated in Figure S1f-l, it is notable that the fiber density of nanoflower-like catalysts increased when the molar ratio of $(NH_4)_2CO_3$ to copper changed from 3 to 3.75 during the preparation. It could be inferred that as enlarging the molar ratio of $(NH_4)_2CO_3$ to copper, the pH value of solution was increased, which would accelerate the hydrolysis of tetraethyl orthosilicate (TEOS) in the beginning of precipitation. In this case, more nuclei underwent growth to form fibers due to the increasing concentration of hydrolyzed TEOS, consequently nanoflower-like structure with fibers of higher density could be fabricated.[35] Additionally, Figure S1e further evidenced the solid sphere structure without obvious open-ended channels of the as-prepared Cu/SiO_2-S, while some lamellar copper silicate appeared on the surface of spheres.

To further demonstrate the pore structure of the catalysts, N_2 adsorption-desorption isotherms and the pore size distribution curves were measured and illustrated in Figure 1. The corresponding specific surface areas and pore properties were summarized in Table S1. As shown in Figure 1a, N_2 physisorption isotherms of all the samples could be assigned to the typical type IV isotherms with H3-type hysteresis loops according to the IUPAC classification, suggesting the

mesoporous structures.[36-37] Notably, the hysteresis loops of the Cu/SiO_2-F samples appeared at comparatively high relative pressure, implying that all the Cu/SiO_2-F catalysts presented large wedge-shaped pores with open ends,[28] which is consistent with their fiber-assembled nanoflower-like morphology. Besides, the pore size distribution curves in Figure 1b for Cu/SiO_2-F catalysts exhibited broad and wide peaks at ca.10~30 nm, which could reflect the distance between assembled fibers.[36] With the increasing molar ratio of $(NH_4)_2CO_3$ to copper, the average pore diameter declined from 22.3 nm of Cu/SiO_2-F-3 to 18.4 nm of Cu/SiO_2-F-3.75, which agrees with the fiber density variation observed from TEM images. Additionally, for the Cu/SiO_2-S sample, it is noticed that there was no obvious N_2 adsorption at the low relative pressure and the specific surface area was small, both indicating that the pores were mainly located on the sphere surface and the solid spherical structure hadn't been dissolved to form micropores. In addition, the pore size distribution curve of Cu/SiO_2-S showed a narrow and sharp peak around 3 nm, which could be ascribed to the formation of lamellar copper silicate, in accordance with the literature.[25] Therefore, the above results of pore properties correspond well to the SEM and TEM results, confirming the success fabrication of nanoflower-like catalysts with different fiber density and the catalyst of solid sphere structure.

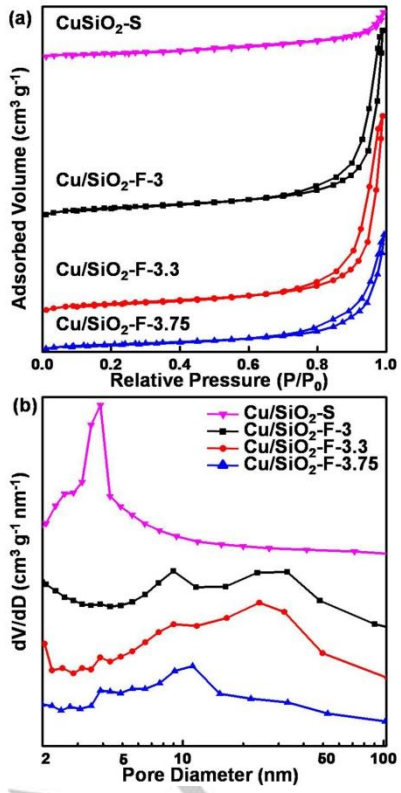

Figure 1. (a) N_2 adsorption-desorption isotherms and (b) pore size distribution curves of the as-prepared catalysts.

Active Copper Species Distribution of the Reduced Catalysts

Copper loadings of the catalysts were detected by inductively coupled plasma optical emission spectrometer (ICP-OES) and listed in Table 1. For the nanoflower-like catalysts, the copper content slightly increased from 17.8 wt.% to 23.3 wt.% when the molar ratio of $(NH_4)_2CO_3$ to copper changed from 3 to 3.75, possibly because the high concentration of ionic ammonium could promote the precipitation of copper ions. The copper loading of Cu/SiO_2-S sample was similar with that of Cu/SiO_2-F-3.75 sample, which were both around 24 wt.%.

Because all the catalysts were first reduced before the reaction, characterization of the reduced catalysts especially for their surface active species distribution was necessary for further study. As shown in Figure 2, both morphology and pore structure of the nanoflower-like samples and the sphere one were not destroyed during the reduction, meanwhile, a lot of nanoparticles appeared among these catalysts. By testing high-resolution TEM, it was found that the lattice fringes of those particles showed the d-spacing of 0.207 nm, which can be ascribed to the (111) plane of metallic copper.[32, 38] The counted copper particle sizes of all the catalysts displayed narrow distributions with most particles of 5 nm approximately. Particularly, with the increase of fiber density, the average copper particle sizes of Cu/SiO_2-F catalysts slightly decreased from 5.2 nm to 4.4 nm. It is worthy pointing out that the average copper particle sizes decreased despite of the increase in copper loadings for a series of Cu/SiO_2-F catalysts, implying that the higher fiber density with stronger metal-support interaction resulting from the increasing pH value and raising concentration of ionic ammonium to copper in the preparation process could effectively enhance the particle dispersion.[39-40]

Powder X-ray diffraction (XRD) patterns of the reduced catalysts are displayed in Figure S2. A broad diffraction peak at approximately 23° of all catalysts was attributed to amorphous SiO_2. The diffraction peaks at 2θ of 43.3°, 50.4°, 74.1° were observed as well in all the reduced catalysts, which should be assigned to the (111), (200) and (220) planes of metallic Cu, respectively.[27] It is noticed that the peaks at 2θ of 43.3° in the diffraction patterns were sharp. According to Scherrer equation, the average metallic copper crystallite sizes of the reduced Cu/SiO_2-F-3, Cu/SiO_2-F-3.3, Cu/SiO_2-F-3.75 catalysts were calculated, which are 11.4 nm, 10.1 nm, 9.9 nm, respectively, while that of Cu/SiO_2-S is 11.5 nm. Comparing the copper particle sizes of the reduced catalysts obtained from XRD and TEM characterizations, it is easy to find the values are quite different. The particle sizes calculated from XRD data are around 10 nm, whereas they are about 5 nm counted from the TEM images. Actually, the poor correlation has been reported several times.[30, 41-42] Although benefiting from the strong metal-support interaction, most the copper particles are about 5 nm as demonstrated, there could be some large ones aggregated in the core areas where the fibers intersected together, which were difficult to be distinguished and counted from the TEM images.[30] And when characterizing the bimodal distribution case, the XRD line broadening analysis alone was not reliable.[41]

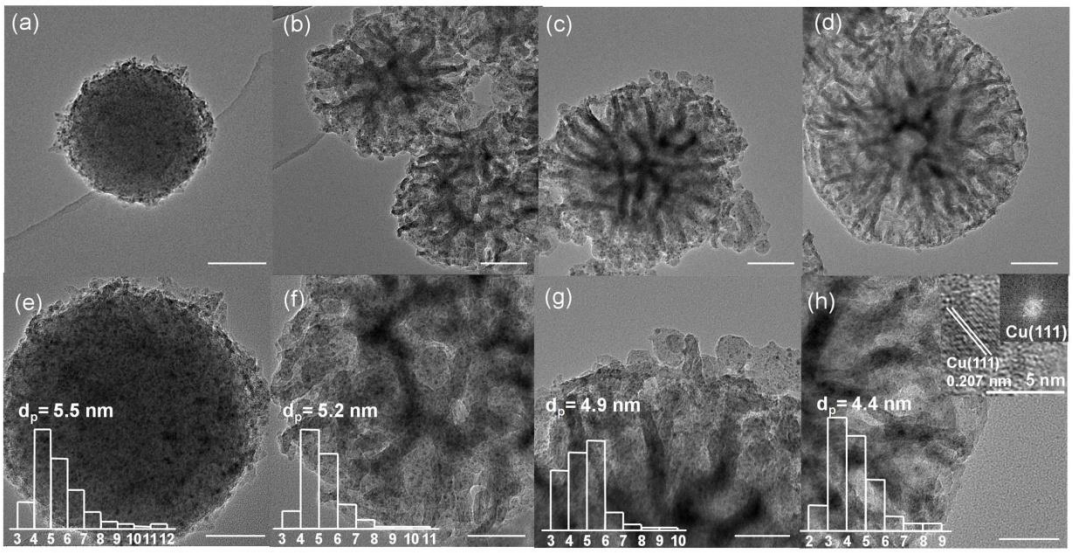

Figure 2. TEM images of the reduced catalysts. (a, e) Cu/SiO_2-S, (b, f) Cu/SiO_2-F-3, (c, g) Cu/SiO_2-F-3.3, (d, h) Cu/SiO_2-F-3.75. Scale bars in (a-d) and (e-h) are 100 nm and 50 nm, respectively. Corresponding Cu particle sizes distribution is shown in the inset.

In this case, we applied N_2O titration to identify the dispersion of copper species quantitatively and accurately. The dispersion (d_{Cu}) and the specific surface area (S_{Cu^0}) of metallic copper are summarized in Table 1 and Table S1. It could be found that when the fiber density of Cu/SiO_2-F catalysts increased, the copper dispersion increased from 10.2% to 15.9%, as well as the specific surface area of metallic copper was improved from 11.7 m^2/g to 23.9 m^2/g. This further confirmed that the high molar ratio of $(NH_4)_2CO_3$ to copper could provide strong metal-support interaction and promote the dispersion of copper species. According to the metal dispersion, the calculated average Cu particle sizes were listed in Table S1. It is indicated that the fibers of nanoflower-like catalysts possibly played an important role during the reduction process as well, of preventing the copper species from aggregation and reducing the average particle sizes. In addition, it is displayed that the Cu dispersion and specific surface area of metallic copper in Cu/SiO_2-S sample were the highest ones among all the samples, possibly due to the spatial confinement effect of lamellar copper silicate during reduction.[43] To further verify the above results, temperature programmed reduction of hydrogen (H_2-TPR) experiments were conducted. As depicted in Figure S3, the main reduction peak of Cu/SiO_2-F-3 sample was situated at 230 °C, and gradually shifted to 223 °C with the increase of fiber density, companied with the narrowing peak width, which could be attributed to the decreased copper particle size and narrowed bimodal size distribution. Additionally, there were two reduction peaks of Cu/SiO_2-S catalyst appeared at 222 °C and 237 °C respectively. The high-temperature one indicated the existence of some large copper particles in the bimodal distribution of Cu/SiO_2-S sample. These results are consistent with all the above characterizations, evidencing the reliable quantitative measurement of metallic copper species.

Thus, it could be summarized that the fibers of high density in the nanoflower-like catalysts could effectively promote the active species dispersion, in which most copper particles located on the surfaces are small, ca.5 nm, while some of large ones might generate between the crossed fibers. Meanwhile the Cu/SiO_2-S as the contrast sample, showed the highest copper loading and surface area of metallic copper species, allowing us to compare their morphology effects on hydrogen adsorption, which is generally considered to be related to the Cu^0 species.

The surface copper chemical states of the reduced catalysts were detected by X-ray photoelectron spectra (XPS) and Auger electron spectroscopy (AES) to analyze the active species distribution. As shown in Figure 3a, two peaks at 932.6 eV and 952.5 eV were assigned to the binding energy of Cu $2p_{3/2}$ and Cu $2p_{1/2}$, respectively.[44] Moreover, no any obvious satellite peak between 942 eV and 944 eV ascribed to Cu^{2+} species, can be observed, implying the complete reduction of Cu^{2+} to Cu^+ or Cu^0 species.[45] Due to the similar binding energy of Cu^+ and Cu^0 species, it is difficult to distinguish them only by the XPS spectra, then Cu LMM AES spectra of the reduced catalysts were collected. As illustrated in Figure 3b, the peaks of all the reduced catalysts were asymmetrical and broad, suggesting the coexistence of Cu^+ and Cu^0 species on the surface. According to the deconvolution results, the two peaks at 573.1 eV and 570.0 eV could be assigned to Cu^+ and Cu^0, respectively.[46] Thus combining with the metallic copper dispersion obtained from N_2O titration, the amount of surface Cu^+ and Cu^0 species can be calculated, under the assumption that Cu^+ and Cu^0 ions occupy the same surface area and have the same atomic sensitivity factor. As shown in Table 1, by increasing the fiber density, Cu/SiO_2-F catalysts exhibited a decreasing proportion of Cu^+ species as well as the surface area declined from 17.0 m^2/g to 12.2 m^2/g. For the Cu/SiO_2-S catalyst, it showed the smallest surface area of Cu^+ species, which might be attributed to the small specific surface area of spheres.[47]

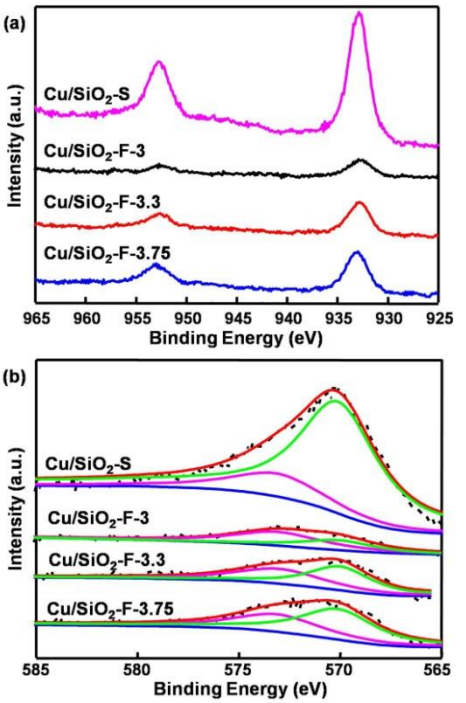

Figure 3. (a) Cu 2p XPS spectra and (b) Cu LMM Auger spectra of the reduced catalysts.

Table 1. Contents and the surface distribution of copper species in the as-prepared catalysts.

Catalyst	Cu loading [a] [wt.%]	S_{Cu^0} [b] [m^2/g]	X_{Cu^+} [c] [%]	S_{Cu^+} [d] [m^2/g]
Cu/SiO_2-S	24.8	29.8	16.5	5.9
Cu/SiO_2-F-3	17.8	11.7	59.2	17.0
Cu/SiO_2-F-3.3	19.1	17.6	47.7	16.1
Cu/SiO_2-F-3.75	23.3	23.9	33.8	12.2

[a] Determined by ICP-OES analysis. [b] Determined by N_2O titration method. [c] $Cu^+/(Cu^+ + Cu^0)$ calculated from Cu LMM AES spectra. [d] Cu^+ surface area obtained with the combination of S_{Cu^0} and X_{Cu^+} assuming Cu^+ and Cu^0 occupy identical areas and have identical atomic sensitivity factors.

To verify the specific surface areas of copper species, all the catalysts were further characterized by in situ Fourier transform infrared spectroscopy (FTIR) of CO absorption,[46] and the results were displayed in Figure 4. Considering that the interaction between CO and Cu^0 or Cu^{2+} species is weak and there are no Cu^{2+} species existed after reduction evidenced by XPS and XRD results, the bands at 2100~2200 cm^{-1} should be ascribed to CO absorbed on the Cu^+ species.[46, 48] As shown in Figure 4, for the Cu/SiO_2-F catalysts, the intensity of the bands increased with the decrease in fiber density, suggesting the increase of surface Cu^+ species. Meanwhile, the intensity band of Cu/SiO_2-S sample was quite weak, indicating a few Cu^+ species existed on the solid sphere surface. To compare the analysis results of surface active copper species obtained by different characterizations, the correlation of calculated surface Cu^+ areas based on Cu LMM AES analysis (S_{Cu^+}) and integral peak areas obtained from the in situ FTIR of CO adsorption (marked as A_{Cu^+}) was exhibited in Figure S4. It is shown a good linear relationship, which indicates the reliable quantitative analysis of surface Cu^0 and Cu^+ species.

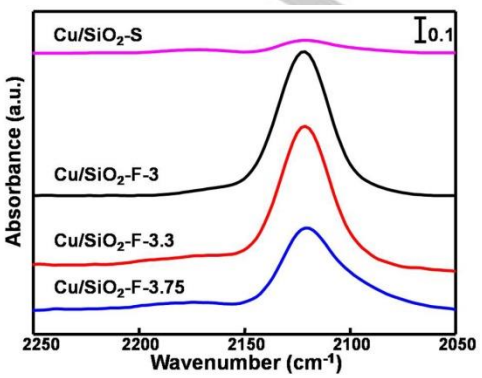

Figure 4. In situ FTIR of CO adsorption spectra of the reduced catalysts.

Catalytic Performance in the EC Hydrogenation

Gas-phase hydrogenation of EC to produce methanol and EG was conducted in a fixed-bed reactor to investigate the catalytic performance of the as-prepared catalysts. The reaction was conducted at 180 °C, 3 MPa of the total system pressure, and H_2/EC ratios varied from 200 to 60. As shown in Figure 5a, all the catalysts achieved almost 100% EC conversion at high H_2/EC ratio of 160 to 200. When the H_2/EC ratio was decreased to 140, the EC conversion of Cu/SiO_2-S catalyst with solid sphere morphology firstly dropped below 98%, while those of Cu/SiO_2-F catalysts still maintained well, implying the significant improvement in catalytic activity by using the nanoflower-like morphology catalysts. As the H_2/EC ratio further decreased, the EC conversion of Cu/SiO_2-S catalyst reduced rapidly as well as the decline in EC conversion of Cu/SiO_2-F-3 and Cu/SiO_2-F-3.3 could be observed at the H_2/EC ratio of 120 and 80 respectively. Notably, the Cu/SiO_2-F-3.75 catalyst with fibers of the highest density continued to exhibit a remarkable high performance with the EC conversion of approximately 98%. Benefiting from the appropriate properties of silica support with few acidic and basic sites, all catalysts showed great selectivity of methanol and EG,[18] around 70% and 99%, respectively. Notably, with the increasing of $Cu^+/(Cu^0+Cu^+)$, methanol selectivity of those as-prepared catalysts slightly increased first and then declined. The highest methanol selectivity of 75% was achieved on the Cu/SiO_2-F-3.75 catalyst at the $Cu^+/(Cu^0+Cu^+)$ of 33.8%, consistent with the literature,[16, 27] which has been reported that appropriate synergetic effect between surface Cu^0 and Cu^+ species contributed to the selective production of methanol.

It has been widely accepted that the surface Cu^0 sites primarily contribute to the H_2 decomposition in ester hydrogenation.[18, 27, 46] As demonstrated above, the Cu/SiO_2-F-3.75 with the highest density of fibers possessed a large surface area of metallic copper species (23.9 m^2/g), which exhibited excellent catalytic performance even at a very low H_2/EC ratio of 60. However, when it comes to the solid sphere-shaped Cu/SiO_2-F-S catalyst with more surface Cu^0 sites of 29.8 m^2/g, the EC conversion dropped rapidly once the H_2/EC ratio was decreased below 140. It is inferred there are other factors influencing the catalytic performance.

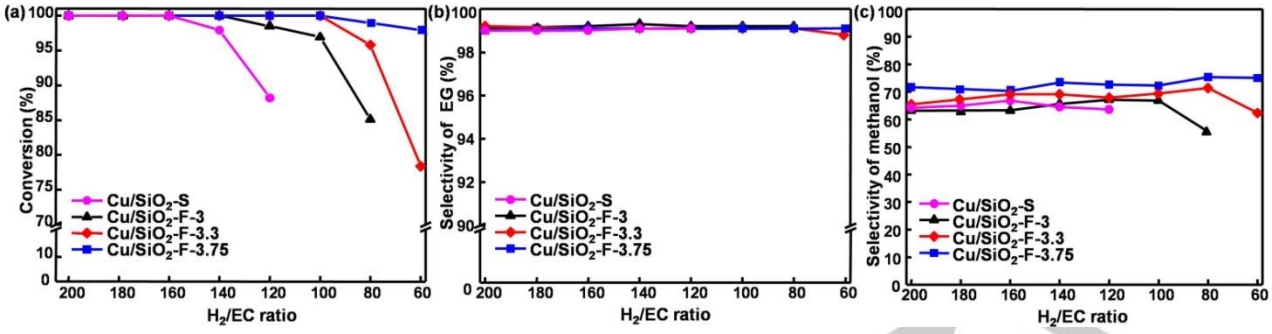

Figure 5. Catalytic performance of the catalysts with different morphologies in the hydrogenation of EC. (a) conversion of EC, (b) selectivity of EG, (c) selectivity of methanol. Reaction conditions: T = 180 °C, P = 3 MPa, $WHSV_{EC}$ = 0.3 h^{-1}.

According to our previous study as well as the literature, the Cu^+ sites could act as electrophilic or Lewis acidic sites to polarize the C=O bond via electron lone pair in oxygen, thus activate the ethylene carbonate, and the synergy effect of Cu^0 and Cu^+ species was crucial for enhancing the catalytic performance of Cu/SiO_2 in the EC hydrogenation.[18, 27, 46] Thus, to gain further insights of the contributions of Cu^0 and Cu^+ species toward the EC hydrogenation, we tested the samples under the same harsh conditions (the H_2/EC ratio was 60) and analyzed their catalytic performance on each Cu species site, denoted as TOF_{Cu^0} and TOF_{Cu^+} shown in Figure S5. The catalytic performance was positive correlated with the surface area of Cu^+ species as reported, implying the contribution of Cu^+ species in the activation of EC.[14, 16, 28] Notably, for the nanoflower-like catalysts, TOF_{Cu^+}, which is calculated based on the corresponding surface amount of Cu^+ sites, was increasingly rising with the increasing number of the Cu^0 sites, instead of a linear correlation. And when it comes to the solid sphere-shaped sample, it exhibited an unexpected drop of TOF_{Cu^+}, indicating there must be some other factors besides the amount of Cu^0 and Cu^+ species greatly affecting the catalytic performance.

Hydrogen-Enrichment Effect of the Nanoflower-like Catalysts

It has been found that the morphology of catalysts could also act as a main contributor to the enhanced catalytic performance. The concave side of curved surface exhibited more strongly interaction with the H_2 molecules than with the convex surface when the distance was equal, which had been calculated by using DFT and Monte Carlo methods in our previous work and literature.[32-33, 49] Accordingly, the better adsorption ability of hydrogen on the concave side of nanoflower fibers than the convex sphere surface could probably be the reason for the difference in catalytic performance.

To explore that, high-pressure hydrogen adsorption measurement was carried out under the reaction temperature of 180 °C. As demonstrated in Figure 6, it is observed that at the reaction pressure of 3 MPa, the H_2-adsorption volume of Cu/SiO_2-F-3.75 was 3.2 mL/g, higher than 2.5 mL/g of the Cu/SiO_2-S. As the pressure increased, the difference in the H_2-adsorption volumes between the two catalysts became more significant. Although the surface area of metallic copper in Cu/SiO_2-F-3.75 sample was not as large as that of the Cu/SiO_2-S catalyst, it possessed a higher adsorption volume of H_2. These results indicated that nanoflower-like structure of Cu/SiO_2-F-3.75 presented a remarkable enhancement of the hydrogen adsorption, probably owing to the dense fiber channels with lots of concave surfaces compared to the solid spherical Cu/SiO_2-S with convex surfaces. Consequently, the hydrogen-enrichment effect could increase the local hydrogen concentration around the active sites on the fibers, further improve the TOF_{Cu^+} as well as the hydrogenation rate and result in the maintained excellent activity even in the feed at a low H_2/EC ratio. Additionally, combining the catalytic performance of other nanoflower-like catalysts, the increasing growth rate of TOF_{Cu^+} as the increased fiber density could also be attributed to the hydrogen-enrichment effect of the concave surfaces of fibers.

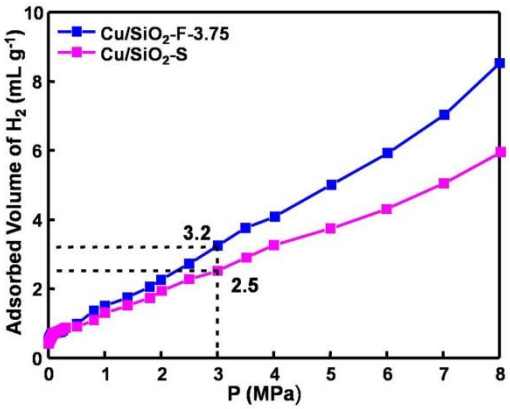

Figure 6. H_2-adsorption isotherms of the Cu/SiO_2-F-3.75 and Cu/SiO_2-S catalysts. Adsorption temperature: 180 °C.

Conclusion

In this work, we report a series of nanoflower-like catalysts prepared via one-step hydrolysis precipitation method. By tuning the molar ratio of ammonium carbonate to copper in the preparation, nanoflower-like catalysts with different fiber density were successfully fabricated. It is demonstrated the Cu/SiO_2-F-3.75 catalyst with fibers of the highest density exhibited the excellent catalytic performance in EC hydrogenation, which enabled the H_2/EC ratio to be reduced to 60 to obtain an EC conversion of approximately 98%, while the contrast sample of silica sphere supported copper catalyst required at least a H_2/EC ratio of 140. The selectivity of methanol (75%) and EG (99%) for the Cu/SiO_2-F-3.75 catalyst were excellent and not greatly influenced by the drop of H_2/EC ratio as well. Combining the

characterizations and analysis of the textural properties and distribution of the active copper species of these catalysts, the effect of nanoflower-like morphology on enhancing the catalytic performance in hydrogenation reaction was revealed. It could be concluded that the nanoflower fibers with high density could effectively enriching the H_2 adsorption, consequently accelerate the hydrogenation rate and keep the performance at the low H_2/EC ratio. These understandings could make an instructive contribution to the further design of catalysts for the industrial application concerning the hydrogenation reactions.

Experimental Section

Catalyst Preparation

The nanoflower-like Cu/SiO_2 catalysts were prepared by one-step hydrolysis precipitation method in the presence of poly(ethylene glycol)-block-poly(propylene glycol)-block-poly(ethylene glycol) (P123, Aldrich) with tetraethyl orthosilicate (TEOS) as silica source.[30, 44] Different catalysts were synthesized by tuning the molar ratio of ammonium carbonate to copper to 3, 3.3, 3.75, respectively. Briefly, a required amount of $Cu(NO_3)_2{\cdot}3H_2O$ and 1.5 g P123 were dissolved in a mixture of 100 mL water and 50 mL ethanol under stirring. Subsequently, ammonium carbonate aqueous was added dropwise into the mixed solution. TEOS of corresponding weight was dropped into the mixture with the same drop velocity. After further stirred for 4 h at 30 °C, the suspension was heated to 80 °C to evaporate ammonia until the pH value reached 6-7. Then, the precipitate was filtered, washed several times with deionized water and ethanol, and dried at 90 °C overnight. The samples were calcined in static air in a muffle furnace at 450 °C for 4 h. Finally, the catalysts were tableted, crushed and sieved to collect 40-60 mesh particles. These catalysts were denoted as Cu/SiO_2-F-x (x means the molar ratio of $(NH_4)_2CO_3$ to copper).

For a comparison, another Cu/SiO_2 catalyst with similar copper loading was synthesized by ammonia evaporation method with solid Stöber spheres as the silica source, denoted as Cu/SiO_2-S. First, to prepare solid spheres, 18 mL ammonia was added into 50 mL deionized water, followed by the addition of a mixture of 9 mL TEOS and ethanol. The mixture was then stirred at 40 °C for 2 h to obtain the solid silica spheres. Afterwards, the spheres were separated by centrifugation and washed by ethanol and deionized water for several times, and redispersed into 45 mL deionized water for the next preparation step. $Cu(NO_3)_2{\cdot}3H_2O$ was dissolved in 100 mL water followed by the addition of 9.8 mL ammonia. Under stirring, the 45 mL dispersed silica spheres solution was added dropwise. Then the mixture was maintained at 30 °C, stirring 4 h. Afterwards the suspension was heated to 80 °C to evaporate ammonia until the pH reached 6-7. Then, the precipitate was filtered, washed with deionized water, and dried overnight at 90 °C, calcined in a muffle furnace at 450 °C for 4 h. Finally, the catalysts were tableted, crushed and sieved to collect 40-60 mesh particles.

Catalyst Characterization

N_2 physisorption analysis was measured at -196 °C by Micromeritics ASAP 2460. Before the measurement, the samples first were degassed at 300 °C for 4 h. The specific surface area and pore size distribution were calculated by the Brunauer-Emmett-Teller (BET) method and the Barrett-Joyner-Halenda (BJH) method based on the adsorption branches of isotherms, respectively.

ICP-OES was applied to determine Cu contents of the catalysts.

XRD was conducted on Rigaku Model C/max-2500 diffractometer equipped with a Cu Kα radiation source (λ= 1.5406 Å). The patterns were obtained from 2θ of 10° to 90° with a rate of 8°/min. All catalysts were first reduced at 300 °C for 4 h, then sealed by N_2 to avoid air oxidation. The particle sizes of catalysts were calculated using the Scherrer equation.

H_2-TPR was performed on a Micromeritics Autochem II 2920 instrument equipped with a thermal conductivity detector (TCD). Briefly, samples were placed into a U-type quartz tube and then pretreated in Ar atmosphere at 200 °C for 1 h to remove water or other absorbed substances. After cooling to ambient temperature, the samples were heated to 800 °C in 10% H_2/Ar at a rate of 10 °C/ min.

SEM images were collected on a Hitachi S4800 field-emission microscope operating at 10.0 kV to observe the overall morphology. TEM images were obtained by JEM-2100F system electron microscope to measure the detailed morphology and structure. The samples were ultrasonically dispersed in ethanol for 20 min, then dropped onto the ultra-thin carbon membrane and dried in air. About 100 nanoparticles were counted to illustrate the average copper particle size distribution.

XPS and AES were carried out on PHI 1600 ESCA with an Al Kα X-ray radiation source (hv = 1486.6 eV). The catalysts were first reduced in a flow of H_2 at 300 °C for 4 h before the measurement. The binding energies were calibrated using the C 1s peak at 284.6 eV as the reference. The experimental errors were within ± 0.2 eV.

N_2O titration combined pulse reduction was used to measure the specific surface area of metallic copper by Micromeritics Autochem II 2920. About 50 mg sample was reduced in H_2 at 300 °C for 1 h, followed by purge and then treating with N_2O flow at 90 °C for 1 h to completely oxidize surface metallic copper to Cu_2O. After purge for 1 h, the sample was then reduced at 300 °C by 10% H_2/Ar pulse titration. The amounts of consumed H_2 during the both reduction steps were monitored by TCD. The Cu dispersion (d_{Cu}) and metallic Cu surface area (S_{Cu}^0) were calculated by the equations described by Zhao et al.[44]

In situ FTIR of CO adsorption was conducted to verify the surface Cu^+ species amount by using a Nicolet 6700 spectrometer. Catalysts were pressed in to self-supporting disks with a certain weight. Then the sample was loaded into the in situ cell and reduced in the flow of 10% H_2/Ar at 300 °C for 1 h. After cooling to 30 °C in He flow, the sample was exposed to CO flow for 30 min. After that, the sample was purged by He, at the same time the spectra were collected until no changes between the latest two spectra.

High-pressure hydrogen adsorption was implemented on a pressure composition isothermal system (Micromeritics ASAP 2050). The sample was reduced at 300 °C in a flow of hydrogen before measurement. Afterwards, a 2 mL stainless steel tube was filled with the reduced sample and linked to the instrument. Pretreatment was taken at 300 °C for 2 h under vacuum in order to remove water and other adsorbed molecules. Subsequently cooled down to the reaction temperature of 180 °C, H_2 was injected gradually to increase the pressure up to 8 MPa, and the isotherms of H_2 adsorption were put on record during this step.

Catalytic Performance Tests

The catalytic performance for the gas-phase hydrogenation of ethylene carbonate was investigated in a stainless-steel fixed-bed reaction system. Typically, 0.8 g catalyst (40-60 mesh) was loaded into a certain region of the tubular reactor where could keep temperature constant. A thermocouple was inserted for the supervision of reaction temperature. The catalyst was first reduced in situ under a flow of H_2 at 300 °C for 4 h. After cooling down to 180 °C, the feed (10 wt.% , EC (> 99%, Aladdin) dissolved in 1,4-dioxane) was continuously pumped into the reaction system at a certain weight hourly space velocity (WHSV). After the reaction was steady under the condition, the liquid products were

collected and analyzed on the Agilent Micro GC 6820 with an HP-INNOWAX capillary column (Hewlett-Packard Company, 30 m × 0.32 mm × 0.50 μm) with a flame ionization detector (FID). Several samples under one experiment condition were taken and analyzed through GC system to ensure the repeatability. The outlet gas was analyzed by the Shimadzu GC 2014C instrument with both TCD and FID detectors.

Acknowledgements

We are grateful for the supports from the National Key R&D Program of China (2018YFB0605803), the National Natural Science Foundation of China (21706184, 21938008), Natural Science Foundation of Tianjin City (18JCQNJC06100) and the National Postdoctoral Program for Innovative Talents of China (BX20180211).

Conflict of Interest

The authors declare no conflict of interest.

Keywords: carbon dioxide • hydrogenation • Cu-based catalyst • hydrogen enrichment • ethylene carbonate

[1] E. M. Fischer, R. Knutti, *Nat. Clim. Change* **2015**, *5*, 560-564.
[2] C. S. Watson, N. J. White, J. A. Church, M. A. King, R. J. Burgette, B. Legresy, *Nat. Clim. Change* **2015**, *5*, 565-568.
[3] H. S. Baker, R. J. Millar, D. J. Karoly, U. Beyerle, B. P. Guillod, D. Mitchell, H. Shiogama, S. Sparrow, T. Woollings, M. R. Allen, *Nat. Clim. Change* **2018**, *8*, 604-608.
[4] M. R. Smith, S. S. Myers, *Nat. Clim. Change* **2018**, *8*, 834-839.
[5] M. Aresta, A. Dibenedetto, A. Angelini, *Chem. Rev.* **2014**, *114*, 1709-1742.
[6] W. Li, H. Wang, X. Jiang, J. Zhu, Z. Liu, X. Guo, C. Song, *RSC Adv.* **2018**, *8*, 7651-7669.
[7] N. A. Bahari, W. N. R. W. Isahak, M. S. Masdar, Z. Yaakob, *Int. J. Energy Res.* **2019**, *43*, 5128-5150.
[8] A. Goeppert, M. Czaun, J. P. Jones, G. K. S. Prakash, G. A. Olah, *Chem. Soc. Rev.* **2014**, *43*, 7995-8048.
[9] S. Dang, H. Yang, P. Gao, H. Wang, X. Li, W. Wei, Y. Sun, *Catal. Today* **2019**, *330*, 61-75.
[10] F. Lin, X. Jiang, N. Boreriboon, Z. Wang, C. Song, K. Cen, *Appl. Catal. A* **2019**, *585*, 117210.
[11] M. Mureddu, F. Ferrara, A. Pettinau, *Appl. Catal. B* **2019**, *258*, 117941.
[12] T. Liu, X. Hong, G. Liu, *ACS Catal.* **2019**, *10*, 93-102.
[13] V. Zubar, Y. Lebedev, L. M. Azofra, L. Cavallo, O. E.-Sepelgy, M. Rueping, *Angew. Chem. Int. Ed.* **2018**, *57*, 13439-13443.
[14] Y. Ding, J. Tian, W. Chen, Y. Guan, H. Xu, X. Li, H. Wu, P. Wu, *Green Chem.* **2019**, *21*, 5414-5426.
[15] Z. Han, L. Rong, J. Wu, L. Zhang, Z. Wang, K. Ding, *Angew. Chem. Int. Ed.* **2012**, *51*, 13041-13045.
[16] W. Chen, T. Song, J. Tian, P. Wu, X. Li, *Catal. Sci. Technol.* **2019**, *9*, 6749-6759.
[17] C. Lian, F. Ren, Y. Liu, G. Zhao, Y. Ji, H. Rong, W. Jia, L. Ma, H. Lu, D. Wang, Y. Li, *Chem. Commun.* **2015**, *51*, 1252-1254.
[18] H. Liu, Z. Huang, Z. Han, K. Ding, H. Liu, C. Xia, J. Chen, *Green Chem.* **2015**, *17*, 4281-4290.
[19] F. Li, L. Wang, X. Han, P. He, Y. Cao, H. Li, *RSC Adv.* **2016**, *6*, 45894-45906.
[20] H. Yue, Y. Zhao, X. Ma, J. Gong, *Chem Soc Rev.* **2012**, *41*, 4218-4244.
[21] J. Ma, N. Sun, X. Zhang, N. Zhao, F. Xiao, W. Wei, Y. Sun, *Catal. Today* **2009**, *148*, 221-231.
[22] M. Cokoja, C. Bruckmeier, B. Rieger, W. A. Herrmann, F. E. Kuhn, *Angew. Chem. Int. Ed.* **2011**, *50*, 8510-8537.
[23] X. Chen, Y. Cui, C. Wen, B. Wang, W.-L. Dai, *Chem. Commun.* **2015**, *51*, 13776-13778.
[24] F. Li, L. Wang, X. Han, Y. Cao, P. He, H. Li, *Int. J. Hydrogen Energy* **2017**, *42*, 2144-2156.
[25] R.-P. Ye, L. Lin, J.-X. Yang, M.-L. Sun, F. Li, B. Li, Y.-G. Yao, *J. Catal.* **2017**, *350*, 122-132.
[26] X. Yu, T. A. Vest, N. Gleason-Boure, S. G. Karakalos, G. L. Tate, M. Burkholder, J. R. Monnier, C. T. Williams, *J. Catal.* **2019**, *380*, 289-296.
[27] F. Deng, N. Li, S. Tang, C. Liu, H. Yue, B. Liang, *Chem. Eng. J.* **2018**, *334*, 1943-1953.
[28] J. Tian, W. Chen, P. Wu, Z. Zhu, X. Li, *Catal. Sci. Technol.* **2018**, *8*, 2624-2635.
[29] J. Kim, N. Pfander, G. Prieto, *ChemSusChem* DOI: 10.1002/cssc.202000166.
[30] C. Zhang, L. Wang, J. Liu, Y. Yang, P. He, Y. Cao, J. Chen, H. Li, *ChemCatChem* **2018**, *10*, 4617-4628.
[31] M. Zhou, Y. Shi, K. Ma, S. Tang, C. Liu, H. Yue, B. Liang, *Ind. Eng. Chem. Res.* **2018**, *57*, 1924-1934.
[32] D. Yao, Y. Wang, Y. Li, Y. Zhao, J. Lv, X. Ma, *ACS Catal.* **2018**, *8*, 1218-1226.
[33] D. Yao, Y. Wang, K. H.-Legault, A. Li, Y. Zhao, J. Lv, S. Huang, X. Ma, *ACS Catal.* **2019**, *9*, 2969-2976.
[34] K. X. Yao, H. C. Zeng, *Chem. Mater.* **2011**, *24*, 140-148.
[35] A. Maity, V. Polshettiwar, *ACS Appl. Nano Mater.* **2018**, *1*, 3636-3643.
[36] M. Ouyang, Y. Wang, J. Zhang, Y. Zhao, S. Wang, X. Ma, *RSC Adv.* **2016**, *6*, 12788-12791.
[37] M. Ouyang, J. Wang, B. Peng, Y. Zhao, S. Wang, X. Ma, *Appl. Surf. Sci.* **2019**, *466*, 592-600.
[38] S. Bai, Q. Shao, P. Wang, Q. Dai, X. Wang, X. Huang, *J. Am. Chem. Soc.* **2017**, *139*, 6827-6830.
[39] S. Xiao, Y. Zhang, P. Gao, L. Zhong, X. Li, Z. Zhang, H. Wang, W. Wei, Y. Sun, *Catal. Today* **2017**, *281*, 327-336.
[40] Q. Xin, A. Papavasiliou, N. Boukos, A. Glisenti, J. P. H. Li, Y. Yang, C. J. Philippopoulos, E. Poulakis, F. K. Katsaros, V. Meynen, P. Cool, *Appl. Catal. B* **2018**, *223*, 103-115.
[41] P. Munnik, M. Wolters, A. Gabrielsson, S. D. Pollington, G. Headdock, J. H. Bitter, P. E. de Jongh, K. P. de Jong, *J. Phys. Chem. C* **2011**, *115*, 14698-14706.
[42] Z. Li, Z. Zeng, D. Yao, S. Fan, S. Guo, J. Lv, S. Huang, Y. Wang, X. Ma, *ACS Sustainable Chem. Eng.* **2019**, *8*, 200-209.
[43] J. Gong, H. Yue, Y. Zhao, S. Zhao, L. Zhao, J. Lv, S. Wang, X. Ma, *J. Am. Chem. Soc.* **2012**, *134*, 13922-13925.
[44] Y. Zhao, S. Li, Y. Wang, B. Shan, J. Zhang, S. Wang, X. Ma, *Chem. Eng. J.* **2017**, *313*, 759-768.
[45] Y. Zhao, B. Shan, Y. Wang, J. Zhou, S. Wang, X. Ma, *Ind. Eng. Chem. Res.* **2018**, *57*, 4526-4534.
[46] Y. Wang, Y. Shen, Y. Zhao, J. Lv, S. Wang, X. Ma, *ACS Catal.* **2015**, *5*, 6200-6208.
[47] Y. Wang, W. Yang, D. Yao, S. Wang, Y. Xu, Y. Zhao, X. Ma, *Catal. Today DOI:* 10.1016/j.cattod.2019.06.031.
[48] J. Zheng, J. Zhou, H. Lin, X. Duan, C. T. Williams, Y. Yuan, *J. Phys. Chem. C* **2015**, *119*, 13758-13766.
[49] J. Guan, X. Pan, X. Liu, X. Bao, *J. Phys. Chem. C* **2009**, *113*, 21687-21692.

Entry for the Table of Contents

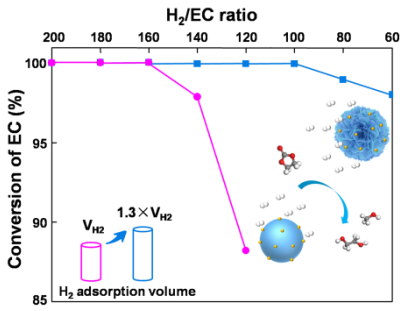

In the hydrogenation of ethylene carbonate (EC), nanoflower-like catalysts with high fiber density exhibited nearly 98% EC conversion when the H_2/EC ratio was decreased to 60, while the catalyst with solid sphere structure required at least a H_2/EC ratio of 140. This is attributed to the H_2-enrichment effect of nanoflower-like morphology with dense fibers, which accelerated the reaction rate and achieved excellent activity at a low H_2/EC ratio.